A SPECTRAL MIMETIC LEAST-SQUARES METHOD FOR THE STOKES EQUATIONS WITH NO-SLIP BOUNDARY CONDITION

MARC GERRITSMA AND PAVEL BOCHEV

Dedicated to Max Gunzburger's 70th birthday.

Abstract Formulation of locally conservative least-squares finite element methods (LSFEM) for the Stokes equations with the no-slip boundary condition has been a long standing problem. Existing LSFEMs that yield exactly divergence free velocities require non-standard boundary conditions [5], while methods that admit the no-slip condition satisfy the incompressibility equation only approximately [6, Chapter 7]. Here we address this problem by proving a new non-standard stability bound for the velocity-vorticity-pressure Stokes system augmented with a no-slip boundary condition. This bound gives rise to a norm-equivalent least-squares functional in which the velocity can be approximated by div-conforming finite element spaces, thereby enabling a locally-conservative approximations of this variable. We also provide a practical realization of the new LSFEM using high-order spectral mimetic finite element spaces [24] and report several numerical tests, which confirm its mimetic properties.

1. Introduction

In this paper we consider least-squares finite element methods (LSFEMs) for the velocity-vorticity-pressure (VVP) formulation of the Stokes problem

$$\left\{\begin{array}{rl} \nabla\times\boldsymbol{\omega}+\nabla p=\boldsymbol{f} & \text{in } \Omega \\ \nabla\times\boldsymbol{u}-\boldsymbol{\omega}=0 & \text{in } \Omega \\ \nabla\cdot\boldsymbol{u}=0 & \text{in } \Omega \end{array}\right. , \tag{1}$$

where $\boldsymbol{u}$ denotes the velocity, $\boldsymbol{\omega}$ the vorticity, p the pressure and $\boldsymbol{f}$ the force per unit mass. Our main focus is on the formulation of conforming LSFEMs that are (i) locally conservative, and (ii) provably stable when the system (1) is augmented with the no-slip (velocity) boundary condition

$$\boldsymbol{u}=0 \quad \text{on } \partial\Omega. \tag{2}$$

Note that (2) is equivalent to a pair of boundary conditions

$$\boldsymbol{u}\cdot\boldsymbol{n}=0 \quad \text{and} \quad \boldsymbol{u}\times\boldsymbol{n}=0 \quad \text{on } \partial\Omega\,, \tag{3}$$

for the normal and tangential components of the velocity field, respectively.

Two factors motivate the choice of (1) as a foundation for our method. Using first-order systems has been a staple in least-squares formulations because it allows one to reduce the regularity requirement on the finite element spaces as well as the condition number of the resulting algebraic problems. A second consideration is the practical importance of the

Date: January 28, 2016.

1991 *Mathematics Subject Classification.* Primary 65N30, 65N35; Secondary 35J20, 35J46.

Key words and phrases. Least-squares, mimetic methods, spectral element method, mass conservation.

This paper is in final form and no version of it will be submitted for publication elsewhere.

vorticity variable in applications where rotational flow dominates the flow dynamics, such as rotor aerodynamics, the flow around wind turbines or wake flows. Methods that can directly control and possibly reduce the error in the vorticity can be of significant value in these applications.

Formulation of conforming LSFEMs that satisfy both (i) and (ii) had been a long-standing challenge. Existing conforming least-squares methods generally fall into one of the following two categories. The LSFEMs in the first category, see e.g., [4, 10], are stable and accurate for (1) with the boundary condition (2) but satisfy $\nabla \cdot \boldsymbol{u} = 0$ only approximately. Conversely, the LSFEMs in the second category; see, e.g., [5], [6, Chapter 7] yield exactly divergence free velocity fields but require the non-standard normal velocity, tangential vorticity boundary condition

$$\boldsymbol{u} \cdot \boldsymbol{n} = 0 \quad \text{and} \quad \boldsymbol{\omega} \times \boldsymbol{n} = 0 \quad \text{on } \partial\Omega\,, \tag{4}$$

i.e., they specify only the first of the two velocity conditions in (3).

Thus far, achieving both stability and exact mass conservation with the velocity boundary condition has been only possible by switching to a non-conforming formulations such as the discontinuous LSFEMs in [8] and [9], or by employing Lagrange multipliers to enforce mass conservation [15]. Of course the latter negates some of the attractive properties of least-squares methods such as symmetric and positive definite algebraic systems, while the former requires careful selection of mesh-dependent weights for the various jump terms and can result in higher condition numbers. In either case, the resulting least-squares methods tend to be less attractive computationally. It should be mentioned that mass conservation in least-squares methods can be strengthened although not satisfied exactly by employing an additional weight for the residual of the continuity equation [16]. Although this approach can partially mitigate the loss of mass conservation it tends to increase the condition number of the resulting system and to reduce the accuracy with which the formulation satisfies the rest of the equations.

In this paper we address formulation of conservative LSFEMs for the VVP Stokes system with (2) by developing a new, non-standard a priory stability bound for this problem. We refer to this bound as "non-standard" because (i) it uses a "weaker" L^2-norm to measure the residual of the momentum equation in (1), instead of a conventional Sobolev space norm, and (ii) it employes a weak curl in the second equation of (1) and a weak grad operator in the first equation of (1). This stability bound gives rise to a norm-equivalent functional, which can be discretized by using div-conforming elements for the velocity field. We show that the resulting LSFEM is both locally conservative and stable for (1)–(2).

We have organized the rest of the paper as follows. Section 2 introduces notation and some necessary background results. Section 3 establishes a non-standard stability bound for the VVP system and Section 4 presents the associated least-squares formulation. Section 5 describes the compatible (mimetic) spectral element spaces, which we use to discretize the least-squares principle and explains how all necessary differential operators can be expressed by operations on the associated degrees-of-freedom. We present numerical results in Section 6 and conclude with some remarks in Section 7.

2. Preliminaries

In what follows $\Omega \subset \mathbb{R}^d$, $d = 2, 3$ is a bounded open region with Lipschitz boundary $\Gamma = \partial\Omega$. We recall the space $L^2(\Omega)$ of all square integrable functions with norm and inner product denoted by $\|\cdot\|_0$ and $(\cdot,\cdot)_0$, respectively, and its subspace $L^2_0(\Omega)$ of all square integrable functions with a vanishing mean. The spaces $H(curl, \Omega)$ and $H(div, \Omega)$ contain

square integrable functions whose curl and divergence are also square integrable. When equipped with the graph norms

$$\|\boldsymbol{\xi}\|^2_{curl} := \|\boldsymbol{\xi}\|^2_0 + \|\nabla\times\boldsymbol{\xi}\|^2_0 \quad \text{and} \quad \|\boldsymbol{v}\|^2_{div} := \|\boldsymbol{v}\|^2_0 + \|\nabla\cdot\boldsymbol{v}\|^2_0 \,,$$

the spaces $H(curl,\Omega)$ and $H(div,\Omega)$ are Hilbert spaces. We recall the subspaces

$$H_0(curl,\Omega) = \{\boldsymbol{v}\in H(curl,\Omega)\,|\,\boldsymbol{v}\times\boldsymbol{n} = 0 \text{ on } \partial\Omega\}\,,$$

$$H_0(div,\Omega) = \{\boldsymbol{v}\in H(div,\Omega)\,|\,\boldsymbol{v}\cdot\boldsymbol{n} = 0 \text{ on } \partial\Omega\}\ ,$$

of $H(curl,\Omega)$ and $H(div,\Omega)$, respectively containing functions whose tangential and normal traces vanish on the boundary.

2.1. **Adjoint operators.** The mimetic least-squares method in this paper requires two additional operators acting on $L^2(\Omega)$ and $H(div,\Omega)$ functions. Their definition follows.

Definition 1. *The adjoint gradient of $p\in L^2(\Omega)$ is the function $\nabla^* p\in H(div,\Omega)$, which satisfies the relation*

$$(\nabla^* p,\boldsymbol{v})_0 := (p,-\nabla\cdot\boldsymbol{v})_0 + \int_{\partial\Omega} p(\boldsymbol{v}\cdot\boldsymbol{n})\,\mathrm{d}S\ ,\quad \forall\boldsymbol{v}\in H(div,\Omega)\ . \tag{5}$$

The adjoint gradient defines a map $\nabla^* : L^2(\Omega)\mapsto H(div,\Omega)$.

The adjoint curl of $\boldsymbol{v}\in H(div,\Omega)$ is the function $\nabla^*\times\boldsymbol{v}\in H(curl,\Omega)$, which satisfies the relation

$$(\nabla^*\times\boldsymbol{v},\boldsymbol{\xi})_0 := (\boldsymbol{v},\nabla\times\boldsymbol{\xi})_0 - \int_{\partial\Omega}\boldsymbol{v}\cdot(\boldsymbol{n}\times\boldsymbol{\xi})\,\mathrm{d}S\ ,\quad \forall\boldsymbol{\xi}\in H(curl,\Omega)\ . \tag{6}$$

The adjoint curl defines a map $\nabla^*\times : H(div,\Omega)\mapsto H(curl,\Omega)$.

Whenever the test functions in (5) and (6) are restricted to $H_0(div,\Omega)$ and $H_0(curl,\Omega)$, respectively, there holds

$$(\nabla^* p,\boldsymbol{v})_0 := (p,-\nabla\cdot\boldsymbol{v})_0 \quad \forall\boldsymbol{v}\in H_0(div,\Omega), \tag{7}$$

and

$$(\nabla^*\times\boldsymbol{v},\boldsymbol{\xi})_0 := (\boldsymbol{v},\nabla\times\boldsymbol{\xi})_0 \quad \forall\boldsymbol{\xi}\in H_0(curl,\Omega)\,, \tag{8}$$

respectively.

2.2. **The velocity space and its decomposition.** An appropriate starting point in the development of locally conservative least-squares finite element methods for (1)–(2) is to consider the velocity as an element of $H(div,\Omega)$. By further restricting the velocity to $H_0(div,\Omega)$ we can subsume the first of the two boundary conditions in (3) into the space definition. However, since $H(div,\Omega)$ functions are not guaranteed to have a well-defined tangential trace, the second, tangential boundary condition can only be imposed in a weak, variational sense. Thus, in what follows we shall seek the velocity solution in the following subspace of $H(div,\Omega)$:

$$\mathcal{D} = \left\{\boldsymbol{v}\in H_0(div,\Omega)\,\Big|\,\int_{\partial\Omega}\boldsymbol{v}\cdot(\boldsymbol{n}\times\boldsymbol{\xi})\,\mathrm{d}S = 0\,,\ \ \forall\boldsymbol{\xi}\in H(curl,\Omega)\right\}.$$

We note that for any $\boldsymbol{v}\in\mathcal{D}$ there holds

$$(\nabla^*\times\boldsymbol{v},\boldsymbol{\xi})_0 := (\boldsymbol{v},\nabla\times\boldsymbol{\xi})_0 \quad \forall\boldsymbol{\xi}\in H(curl,\Omega)\ . \tag{9}$$

In this work we use the Hodge-Morrey-Friedrichs decomposition of vector fields; see, e.g., [29, Theorem 2.4.2, p.81], [21], and [2]. This result states that every vector field $\boldsymbol{v} \in L^2(\Omega)^d$ has an L^2-orthogonal decomposition

$$\boldsymbol{v} = \boldsymbol{v}_c + \boldsymbol{v}_d + \boldsymbol{h}, \tag{10}$$

into an irrotational, a solenoidal and a harmonic component such that

$$\begin{cases} \nabla \times \boldsymbol{v}_c = 0, & \nabla \cdot \boldsymbol{v}_d = 0 \quad \text{in } \Omega \\ \boldsymbol{n} \times \boldsymbol{v}_c = 0, & \boldsymbol{n} \cdot \boldsymbol{v}_d = 0 \quad \text{on } \Gamma \end{cases} \quad \text{and} \quad \begin{cases} \nabla \times \boldsymbol{h} = 0 \\ \nabla \cdot \boldsymbol{h} = 0 \end{cases} \quad \text{in } \Omega.$$

The harmonic component $\boldsymbol{h}$ can be further decomposed as

$$\boldsymbol{h} = \boldsymbol{h}_c + \boldsymbol{h}_d, \qquad \boldsymbol{n} \times \boldsymbol{h}_c = 0 \quad \text{and} \quad \boldsymbol{n} \cdot \boldsymbol{h}_d = 0 \quad \text{on } \Gamma. \tag{11}$$

By combining the terms from (10) and (11) we obtain an alternative decomposition

$$\boldsymbol{v} = \tilde{\boldsymbol{v}}_c + \tilde{\boldsymbol{v}}_d \tag{12}$$

in which the irrotational and the solenoidal components are given by

$$\tilde{\boldsymbol{v}}_c = \boldsymbol{v}_c + \boldsymbol{h}_c \quad \text{and} \quad \tilde{\boldsymbol{v}}_d = \boldsymbol{v}_d + \boldsymbol{h}_d,$$

respectively. We note that unlike (10) the decomposition (12) is not L^2-orthogonal and so we refer to the latter as the algebraic decomposition of $\boldsymbol{v}$.

Given a vector field $\boldsymbol{v} \in H(div, \Omega)$ it is straightforward to show that its algebraic decomposition satisfies

$$\begin{cases} \boldsymbol{n} \cdot \tilde{\boldsymbol{v}}_c &= \boldsymbol{n} \cdot \boldsymbol{v} \\ \boldsymbol{n} \times \tilde{\boldsymbol{v}}_c &= 0 \end{cases} \quad \text{and} \quad \begin{cases} \boldsymbol{n} \cdot \tilde{\boldsymbol{v}}_d &= 0 \\ \boldsymbol{n} \times \tilde{\boldsymbol{v}}_d &= \boldsymbol{n} \times \boldsymbol{v} \end{cases},$$

where the tangential boundary conditions are understood in a weak sense. It follows that for any $\boldsymbol{v} \in \mathcal{D}$ there holds

$$\boldsymbol{v} = \tilde{v}_c + \tilde{\boldsymbol{v}}_d, \quad \tilde{\boldsymbol{v}}_c, \tilde{\boldsymbol{v}}_d \in \mathcal{D}. \tag{13}$$

In other words, both components of the algebraic decomposition of a vector field $\boldsymbol{v} \in \mathcal{D}$ belong in the same space as $\boldsymbol{v}$. Therefore, we can write $\mathcal{D}$ as an algebraic sum

$$\mathcal{D} = \mathcal{D}_c + \mathcal{D}_d \tag{14}$$

of an irrotational subspace $\mathcal{D}_c$ and a solenoidal subspace $\mathcal{D}_d$.

3. Non-standard stability bound

In this section we establish an a priori stability bound for the VVP Stokes system (1) with the no-slip boundary condition (3). The proof draws upon the techniques in [5] with one important distinction. Stability proof in that paper relies on the orthogonality between $\nabla \times \boldsymbol{\omega}$ and $\nabla^* p$ when $\boldsymbol{\omega}$ has a vanishing tangential component, i.e., the fact that

$$(\nabla \times \boldsymbol{\omega}, \nabla^* p) = 0 \quad \forall \boldsymbol{\omega} \in H_0(curl, \Omega) \quad \text{and} \quad p \in L^2(\Omega)\,. \tag{15}$$

This implies a trivial lower bound (in fact an identity) for the L^2-norm of the residual of the momentum equation

$$\|\nabla \times \boldsymbol{\omega} + \nabla^* p\|_0^2 \geq \|\nabla \times \boldsymbol{\omega}\|_0^2 + \|\nabla^* p\|_0^2\,, \tag{16}$$

which represents a key juncture in the proof.

However, for the case of the no-slip boundary condition of interest to us, for $\boldsymbol{\omega} \in H(curl, \Omega)$ the field $\nabla \times \boldsymbol{\omega}$ is not orthogonal to $\nabla^* p$. As a result, (15), resp. (16) do not hold. Nonetheless, using the algebraic decomposition (14) of the velocity space $\mathcal{D}$ we

are able to prove an analogous result, but in a "weaker" L^2-norm. We define this norm for any $\boldsymbol{u} \in H(div, \Omega)$ according to

$$\|\boldsymbol{u}\|_{\mathcal{D}} = \sup_{\boldsymbol{v} \in \mathcal{D}} \frac{(\boldsymbol{u}, \boldsymbol{v})_0}{\|\boldsymbol{v}\|_0}. \tag{17}$$

Since $\mathcal{D} \subset L^2(\Omega)^d$ the norm (17) can indeed be thought of as a "weaker" L^2-norm.

Our proof relies critically upon the fact that, although the components of the algebraic decomposition (14) are not mutually orthogonal, they are orthogonal to the ranges of $\nabla\times$ and ∇^*, respectively, i.e., for any $\boldsymbol{\omega} \in H(curl, \Omega)$ and $p \in L^2(\Omega)$ there holds

$$(\nabla \times \boldsymbol{\omega}, \boldsymbol{v}_c)_0 = 0 \quad \forall \boldsymbol{v}_c \in \mathcal{D}_c \quad \text{and} \quad (\nabla^* p, \boldsymbol{v}_d)_0 = 0 \quad \forall \boldsymbol{v}_d \in \mathcal{D}_d,$$

respectively. Among other things, this orthogonality implies that

$$\|\nabla \times \boldsymbol{\omega}\|_{\mathcal{D}} = \sup_{\boldsymbol{v} \in \mathcal{D}} \frac{(\nabla \times \boldsymbol{\omega}, \boldsymbol{v})_0}{\|\boldsymbol{v}\|_0} = \sup_{\boldsymbol{v}_d \in \mathcal{D}_d} \frac{(\nabla \times \boldsymbol{\omega}, \boldsymbol{v}_d)_0}{\|\boldsymbol{v}_d\|_0}\,, \tag{18}$$

for all $\boldsymbol{\omega} \in H(curl, \Omega)$, and that

$$\|\nabla^* p\|_{\mathcal{D}} = \sup_{\boldsymbol{v} \in \mathcal{D}} \frac{(\nabla^* p, \boldsymbol{v})_0}{\|\boldsymbol{v}\|_0} = \sup_{\boldsymbol{v}_c \in \mathcal{D}_c} \frac{(\nabla^* p, \boldsymbol{v}_c)_0}{\|\boldsymbol{v}_c\|_0} \tag{19}$$

for all $p \in L^2(\Omega)$. Using (18)–(19) the following theorem establishes a stability bound similar to (16) but in terms of the weaker L^2-norm defined by (17).

Theorem 1. *For all $\boldsymbol{\omega} \in H(curl, \Omega)$ and all $p \in L^2(\Omega)$ there holds*

$$\|\nabla \times \boldsymbol{\omega} + \nabla^* p\|_{\mathcal{D}}^2 \geq \frac{1}{2}\|\nabla \times \boldsymbol{\omega}\|_{\mathcal{D}}^2 + \frac{1}{2}\|\nabla^* p\|_{\mathcal{D}}^2\,. \tag{20}$$

Proof. In order to bound the left-hand side in (20) from below we first use that $\mathcal{D}_d$ is a subspace of $\mathcal{D}$ together with the fact that $\nabla^* p \perp \mathcal{D}_d$ and (18) to obtain

$$\begin{aligned} \|\nabla \times \boldsymbol{\omega} + \nabla^* p\|_{\mathcal{D}} &= \sup_{\boldsymbol{v} \in \mathcal{D}} \frac{(\nabla \times \boldsymbol{\omega} + \nabla^* p, \boldsymbol{v})_0}{\|\boldsymbol{v}\|_0} \geq \sup_{\boldsymbol{v}_d \in \mathcal{D}_d} \frac{(\nabla \times \boldsymbol{\omega} + \nabla^* p, \boldsymbol{v}_d)_0}{\|\boldsymbol{v}_d\|_0} \\ &= \sup_{\boldsymbol{v}_d \in \mathcal{D}_d} \frac{(\nabla \times \boldsymbol{\omega}, \boldsymbol{v}_d)_0}{\|\boldsymbol{v}_d\|_0} \overset{(18)}{=} \|\nabla \times \boldsymbol{\omega}\|_{\mathcal{D}}\,. \end{aligned} \tag{21}$$

Similarly, using that $\mathcal{D}_c$ is a subspace of $\mathcal{D}$ together with $\nabla \times \boldsymbol{\omega} \perp \mathcal{D}_c$ and (19) yields the bound

$$\begin{aligned} \|\nabla \times \boldsymbol{\omega} + \nabla^* p\|_{\mathcal{D}} &= \sup_{\boldsymbol{v} \in \mathcal{D}} \frac{(\nabla \times \boldsymbol{\omega} + \nabla^* p, \boldsymbol{v})_0}{\|\boldsymbol{v}\|_0} \geq \sup_{\boldsymbol{v}_c \in \mathcal{D}_c} \frac{(\nabla \times \boldsymbol{\omega} + \nabla^* p, \boldsymbol{v}_c)_0}{\|\boldsymbol{v}_c\|_0} \\ &= \sup_{\boldsymbol{v}_c \in \mathcal{D}_c} \frac{(\nabla^* p, \boldsymbol{v}_c)_0}{\|\boldsymbol{v}_c\|_0} \overset{(19)}{=} \|\nabla^* p\|_{\mathcal{D}}\,. \end{aligned} \tag{22}$$

Squaring both sides of the bounds in (21–22) preserves the sense of the inequality. Combination of the squared bounds then completes the proof:

$$\begin{aligned} \|\nabla \times \boldsymbol{\omega} + \nabla^* p\|_{\mathcal{D}}^2 &= \frac{1}{2}\|\nabla \times \boldsymbol{\omega} + \nabla^* p\|_{\mathcal{D}}^2 + \frac{1}{2}\|\nabla \times \boldsymbol{\omega} + \nabla^* p\|_{\mathcal{D}}^2 \\ &\overset{(21,22)}{\geq} \frac{1}{2}\|\nabla \times \boldsymbol{\omega}\|_{\mathcal{D}}^2 + \frac{1}{2}\|\nabla^* p\|_{\mathcal{D}}^2\,. \end{aligned}$$

□

To state the main result of this section we introduce the "weak" $H(curl, \Omega)$ norm

$$\|\boldsymbol{\omega}\|_C^2 := \|\boldsymbol{\omega}\|_0^2 + \|\nabla \times \boldsymbol{\omega}\|_{\mathcal{D}}^2.$$

Theorem 2. *There exists a constant $C > 0$ such that*

$$\|\nabla \times \omega + \nabla^* p\|_{\mathcal{D}}^2 + \|\omega - \nabla^* \times \boldsymbol{u}\|_0^2 + \|\nabla \cdot \boldsymbol{u}\|_0^2 \geq C \left\{ \|\omega\|_C^2 + \|\boldsymbol{u}\|_{div} + \|\nabla^* p\|_{\mathcal{D}}^2 \right\} .$$

for every $\boldsymbol{u} \in \mathcal{D}$, $\omega \in H(curl, \Omega)$ and $p \in L_0^2(\Omega)$.

Proof. The proof follows the ideas in [5]. We have

$$\|\nabla^* \times \boldsymbol{u} - \omega\|_0^2 = \|\nabla^* \times \boldsymbol{u}\|_0^2 + \|\omega\|_0^2 - 2(\nabla^* \times \boldsymbol{u}, \omega)_0. \tag{23}$$

To bound the last term we split it in two equal parts. On the one hand, the Cauchy-Schwartz inequality gives the bound

$$(\nabla^* \times \boldsymbol{u}, \omega)_0 \leq \|\nabla^* \times \boldsymbol{u}\|_0 \|\boldsymbol{\omega}\|_0 .$$

On the other hand, by taking into account that $\boldsymbol{u} \in \mathcal{D}$, using the identity (9) and the definition of the weak semi norm (18) we obtain

$$(\nabla^* \times \boldsymbol{u}, \boldsymbol{\omega})_0 = (\boldsymbol{u}, \nabla \times \boldsymbol{\omega})_0 \leq \|\boldsymbol{u}\|_0 \|\nabla \times \boldsymbol{\omega}\|_{\mathcal{D}}.$$

Using the last two inequalities in (23) then gives the bound

$$\|\nabla^* \times \boldsymbol{u} - \omega\|_0^2 \geq \|\nabla^* \times \boldsymbol{u}\|_0^2 + \|\omega\|_0^2 - \|\nabla^* \times \boldsymbol{u}\|_0 \|\omega\|_0 - \|\boldsymbol{u}\|_0 \|\nabla \times \omega\|_{\mathcal{D}} .$$

Application of the ϵ-inequality to the last two terms gives

$$\begin{aligned} &\|\nabla^* \times \boldsymbol{u} - \omega\|_0^2 \\ &\qquad \geq \left(1 - \frac{\delta}{2}\right) \|\nabla^* \times \boldsymbol{u}\|_0^2 + \left(1 - \frac{1}{2\delta}\right) \|\omega\|_0^2 - \frac{\epsilon}{2} \|\boldsymbol{u}\|_0^2 - \frac{1}{2\epsilon} \|\nabla \times \omega\|_{\mathcal{D}}^2 , \end{aligned} \tag{24}$$

while the Poincaré-Friedrichs inequality [6, Theorems A.10-A.11]

$$\|\nabla^* \times \boldsymbol{u}\|_0^2 + \|\nabla \cdot \boldsymbol{u}\|_0^2 \geq \frac{1}{C_P^2} \|\boldsymbol{u}\|_0^2 , \tag{25}$$

allows us to conclude that

$$\begin{aligned} \|\nabla^* \times \boldsymbol{u} - \omega\|_0^2 + \|\nabla \cdot \boldsymbol{u}\|_0^2 \geq{}& \frac{1}{2} (1 - \delta) \|\nabla^* \times \boldsymbol{u}\|_0^2 + \frac{1}{2} \|\nabla \cdot \boldsymbol{u}\|_0^2 \\ &+ \left(1 - \frac{1}{2\delta}\right) \|\omega\|_0^2 + \frac{1}{2} \left(\frac{1}{C_P^2} - \epsilon \right) \|\boldsymbol{u}\|_0^2 - \frac{1}{2\epsilon} \|\nabla \times \omega\|_{\mathcal{D}}^2 . \end{aligned} \tag{26}$$

Adding β times the momentum equation and using Theorem 1 yields

$$\begin{aligned} &\beta \|\nabla \times \omega + \nabla^* p\|_{\mathcal{D}}^2 + \|\nabla^* \times \boldsymbol{u} - \omega\|_0^2 + \|\nabla \cdot \boldsymbol{u}\|_0^2 \\ &\qquad \geq \frac{1}{2} (1 - \delta) \|\nabla^* \times \boldsymbol{u}\|_0^2 + \frac{1}{2} \|\nabla \cdot \boldsymbol{u}\|_0^2 + \left(1 - \frac{1}{2\delta}\right) \|\omega\|_0^2 + \\ &\qquad \frac{1}{2} \left(\frac{1}{C_P^2} - \epsilon \right) \|\boldsymbol{u}\|_0^2 + \frac{1}{2} \left(\beta - \frac{1}{\epsilon} \right) \|\nabla \times \omega\|_{\mathcal{D}}^2 + \frac{\beta}{2} \|\nabla^* p\|_{\mathcal{D}}^2 . \end{aligned} \tag{27}$$

Choosing $\epsilon = 1/C_P^2$, $\delta = 2/3$ and $\beta = 1 + C_P^2$ then gives

$$\begin{aligned} &(1 + C_P^2) \|\nabla \times \omega + \nabla^* p\|_{\mathcal{D}}^2 + \|\nabla^* \times \boldsymbol{u} - \omega\|_0^2 + \|\nabla \cdot \boldsymbol{u}\|_0^2 \\ &\qquad \geq \frac{1}{6} \|\nabla^* \times \boldsymbol{u}\|_0^2 + \frac{1}{2} \|\nabla \cdot \boldsymbol{u}\|_0^2 + \frac{1}{4} \|\omega\|_0^2 + \frac{1}{2} \|\nabla \times \omega\|_{\mathcal{D}}^2 + \frac{1}{2} \left(1 + C_P^2\right) \|\nabla^* p\|_{\mathcal{D}}^2 \\ &\qquad \geq \min \left\{ \frac{1}{6}, \frac{1}{2} \left(1 + C_P^2\right) \right\} \left(\|\omega\|_C^2 + \|\boldsymbol{u}\|_{div}^2 + \|\nabla^* p\|_D^2 \right) . \end{aligned} \tag{28}$$

It follows that

$$\begin{aligned}&\|\omega - \nabla^* \times \boldsymbol{u}\|_0^2 + \|\nabla \times \omega + \nabla^* p\|_{\mathcal{D}}^2 + \|\nabla \cdot \boldsymbol{u}\|_0^2 \\ &\qquad \geq \frac{1}{1+C_P^2}\left[(1+C_P^2)\|\nabla \times \omega + \nabla^* p\|_{\mathcal{D}}^2 + \|\nabla^* \times \boldsymbol{u} - \omega\|_0^2 + \|\nabla \cdot \boldsymbol{u}\|_0^2\right],\end{aligned} \tag{29}$$

which completes the proof. □

4. A least-squares principle

The stability bound in Theorem 2 asserts that

$$\mathcal{J}(\boldsymbol{\xi}, \boldsymbol{v}, q; \boldsymbol{f}) := \frac{1}{2}\left(\|\nabla^* \times \boldsymbol{v} - \boldsymbol{\xi}\|_0^2 + \|\nabla \times \boldsymbol{\xi} + \nabla^* q - \boldsymbol{f}\|_{\mathcal{D}}^2 + \|\nabla \cdot \boldsymbol{v}\|_0^2\right) \tag{30}$$

is a norm-equivalent least-squares functional for $(\boldsymbol{\xi}, \boldsymbol{v}, q) \in \mathcal{X} = H(curl, \Omega) \times \mathcal{D} \times L_0^2(\Omega)$. It follows that the least-squares principle

$$(\boldsymbol{\omega}, \boldsymbol{u}, p) = \arg \min_{(\boldsymbol{\xi}, \boldsymbol{v}, q) \in \mathcal{X}} \mathcal{J}(\boldsymbol{\xi}, \boldsymbol{v}, q; \boldsymbol{f}) \tag{31}$$

is a well-posed minimization problem; see [6]. By setting the first variations of $\mathcal{J}(\boldsymbol{\xi}, \boldsymbol{v}, q; \boldsymbol{f})$ with respect to $\boldsymbol{\xi}$, $\boldsymbol{v}$ and q to zero we obtain the associated Euler-Lagrange equation for (31): seek $(\boldsymbol{\omega}, \boldsymbol{u}, p) \in \mathcal{X}$ such that

$$\begin{aligned}(\nabla \times \boldsymbol{\omega} + \nabla^* p, \nabla \times \boldsymbol{\xi})_{\mathcal{D}} + (\boldsymbol{\omega} - \nabla^* \times \boldsymbol{u}, \boldsymbol{\xi})_0 &= (\boldsymbol{f}, \nabla \times \boldsymbol{\xi})_{\mathcal{D}} && \forall \boldsymbol{\xi} \in H(curl, \Omega) \\ (\nabla^* \times \boldsymbol{u} - \boldsymbol{\omega}, \nabla^* \times \boldsymbol{v})_0 + (\nabla \cdot \boldsymbol{u}, \nabla \cdot \boldsymbol{v})_0 &= 0 && \forall \boldsymbol{v} \in \mathcal{D} \\ (\nabla \times \boldsymbol{\omega} + \nabla^* p, \nabla^* q)_{\mathcal{D}} &= (\boldsymbol{f}, \nabla^* q)_{\mathcal{D}} && \forall q \in L_0^2(\Omega).\end{aligned} \tag{32}$$

The norm-equivalence of the least-squares functional (30) implies that the bilinear form corresponding to (32) is strongly coercive (V-elliptic) on $\mathcal{X} \times \mathcal{X}$.

To discretize (31) we consider conforming finite element subspaces $\mathbf{C}^h \subset H(curl, \Omega)$, $\mathbf{D}_0^h \subset \mathcal{D}$ and $S^h \subset L_0^2(\Omega)$ and set $\mathcal{X}^h = \mathbf{C}^h \times \mathbf{D}_0^h \times S^h$. Following the same arguments as in [5] one can show that the stability bound in Theorem 2 continues to hold on $\mathcal{X}^h$, i.e., the least-squares functional (30) remains norm-equivalent on $\mathcal{X}^h$. As a result, the discrete least-squares principle

$$(\boldsymbol{\omega}^h, \boldsymbol{u}^h, p^h) = \arg \min_{(\boldsymbol{\xi}^h, \boldsymbol{v}^h, q^h) \in \mathcal{X}^h} \mathcal{J}(\boldsymbol{\xi}^h, \boldsymbol{v}^h, q^h; \boldsymbol{f}) \tag{33}$$

is well-posed and the discrete optimality system: seek $(\boldsymbol{\omega}^h, \boldsymbol{u}^h, p^h) \in \mathcal{X}^h$ such that

$$\begin{aligned}\left(\nabla \times \boldsymbol{\omega}^h + \nabla^* p^h, \nabla \times \boldsymbol{\xi}^h\right)_{\mathcal{D}} + \left(\boldsymbol{\omega}^h - \nabla^* \times \boldsymbol{u}^h, \boldsymbol{\xi}^h\right)_0 &= \left(\boldsymbol{f}, \nabla \times \boldsymbol{\xi}^h\right)_{\mathcal{D}} && \forall \boldsymbol{\xi}^h \in \mathbf{C}^h \\ \left(\nabla^* \times \boldsymbol{u}^h - \boldsymbol{\omega}^h, \nabla^* \times \boldsymbol{v}^h\right)_0 + \left(\nabla \cdot \boldsymbol{u}^h, \nabla \cdot \boldsymbol{v}^h\right)_0 &= 0 && \forall \boldsymbol{v}^h \in \mathbf{D}_0^h \\ \left(\nabla \times \boldsymbol{\omega}^h + \nabla^* p^h, \nabla^* q^h\right)_{\mathcal{D}} &= \left(\boldsymbol{f}, \nabla^* q^h\right)_{\mathcal{D}} && \forall q^h \in S^h.\end{aligned} \tag{34}$$

has a unique solution. Moreover, once a basis for $\mathcal{X}^h$ is selected, it is not hard to see that (34) is equivalent to a linear algebraic system for the coefficient vector of $(\boldsymbol{\omega}^h, \boldsymbol{u}^h, p^h)$ having a symmetric and positive definite matrix.

In the next section we construct a conforming spectral element subspace of $\mathcal{X}$. A notable feature of our approach is a choice of degrees of freedom, which allow to combine spectral accuracy with the ability to decompose the differential operators in (34) into a purely topological part and a metric dependent part. This should be contrasted with the approaches in, e.g., [1, 17], which do not allow for such a separation.

5. Mimetic spectral element method

Classical low-order mimetic methods [7] admit factorization of the discrete differential operators into a purely topological and a metric dependent parts. The purely topological part is independent of the size or shape of the mesh or the order of the basis and is responsible for ensuring the validity of vector calculus identities such as $\nabla \times \nabla = 0$ and $\nabla \cdot \nabla \times = 0$. Conversely, the metric-dependent part is responsible for the accuracy of the scheme but it depends on the size and shape of the mesh and the order of the basis. Factorization of discrete operators into such parts induces analogous factorizations of their algebraic representations into products of Gramm-like matrices of the finite element bases and incidence matrices, whose entries contain only the numbers $1, -1$ and 0. Among other things, we use these matrix factorizations to prove the mimetic properties of our method.

Although, besides aiding in the proof of mimetic properties, such factorizations can bring about significant other computational benefits, very few attempts had been made to extend such ideas to higher-order representations. Apart from [3, 23, 24, 27, 28] , the authors are not aware of any other work in that direction.

In this section we will present the spectral element basis functions which span the finite dimensional spaces $\mathbf{C}^h$, $\mathbf{D}_0^h$, $\mathbf{D}^h$ and S^h, as well as the equivalent matrix form of (34) for the two-dimensional case. Using this algebraic representation we derive the discrete conservation properties such as local mass conservation and the fact that the integrated vorticity will always vanish by using the above mentioned factorizations.

Similar ideas can be found in Tonti, [31, 32], Bossavit, [12, 13], Desbrun et al., [18], Bochev et al, [3, 7], Lipnikov et al, [26], Seslija et al., [30], Bonelle and Ern, [11], Lemoine et al., [25], Kreeft et al., [23, 24], Palha et al., [27] and references therein.

5.1. One dimensional basis spectral basis functions.

Consider the interval $[-1, 1] \subset \mathbb{R}$ and the Legendre polynomials, $L_N(\xi)$ of degree N, $\xi \in [-1, 1]$. The $(N + 1)$ roots, ξ_i, of the polynomial $(1 - \xi^2)L'_N(\xi)$ satisfy $-1 \leq \xi_i \leq 1$. Here $L'_N(\xi)$ is the derivative of the Legendre polynomial. The zeros are called the *Gauss-Lobatto-Legendre (GLL) points*. Let $h_i(\xi)$ be the Lagrange polynomial through the GLL points such that

$$h_i(\xi_j) = \begin{cases} 1 & \text{if } i = j \\ 0 & \text{if } i \neq j \end{cases} \qquad i, j = 0, \ldots N \; . \tag{35}$$

The explicit form of the Lagrange polynomials in terms of the Legendre polynomials is given by

$$h_i(\xi) = \frac{(1 - \xi^2)L'_N(\xi)}{N(N + 1)L_N(\xi_i)(\xi_i - \xi)} \; . \tag{36}$$

Let $f(\xi)$ be defined for $\xi \in [-1, 1]$ by

$$f(\xi) = \sum_{i=0}^{N} a_i h_i(\xi) \; . \tag{37}$$

Using property (35) we see that $f(\xi_j) = a_j$, so the expansion coefficients in (37) coincide with the value of f in the GLL nodes. We will refer to this expansion as a *nodal expansion*. The nodal basis functions $h_i(\xi)$ are polynomials of degree N.

The derivatives of the nodal basis functions define another set of functions $e_i(\xi)$ given by

$$e_i(\xi) = -\sum_{k=0}^{i-1} \frac{dh_k(\xi)}{d\xi} \, \mathrm{d}\xi = -\sum_{k=0}^{i-1} \mathrm{d}h_k(\xi) \; . \tag{38}$$

The functions $e_i(\xi)$ are polynomials of degree $(N-1)$, which satisfy [22, 24]

$$\int_{\xi_{j-1}}^{\xi_j} e_i(\xi) = \begin{cases} 1 & \text{if } i = j \\ 0 & \text{if } i \neq j \end{cases} \qquad i, j = 1, \dots N \,. \tag{39}$$

Similar to (37) consider an expansion

$$f(\xi) = \sum_{i=1}^{N} b_i e_i(\xi) \,, \tag{40}$$

in terms of the functions e_i. Using (39) we find that

$$\int_{\xi_{j-1}}^{\xi_j} f(\xi) = b_j \,.$$

that is, the expansion coefficients b_i in this case correspond to the integral of f along the edge $[\xi_{i-1}, \xi_i]$. Accordingly, we call e_i *edge functions* and refer to (40) as an *edge expansion*, see for instance [3, 23, 24, 27] for examples of nodal and edge expansions.

The relationship (38) between nodal and edge functions implies that the derivative of a nodal expansion (37) is an edge expansion (40) [22, 24], that is,

$$f'(\xi) = \sum_{i=0}^{N} a_i h_i'(\xi) = \sum_{i=1}^{N} (a_i - a_{i-1}) e_i(\xi) \,. \tag{41}$$

Remark 1. *Note that the set of polynomials $\{h_i'\}$, $i = 0, \dots, N$ is linearly dependent and therefore does not form a basis, whereas the set $\{e_i\}$, $i = 1, \dots, N$ is linearly independent and therefore forms a basis for the derivatives of the nodal expansion (37).*

For all integrals we use Gauss-Lobatto integration

$$\int_{-1}^{1} f(\xi) \, \mathrm{d}\xi \approx \sum_{i=0}^{N} f(\xi_i) w_i \,, \tag{42}$$

where the Gauss-Lobatto weight are given by

$$w_i = \frac{2}{N(N+1) L_N^2(\xi_i)} \quad \text{for } i = 0, \dots, N \,. \tag{43}$$

Gauss-Lobatto integration is exact for polynomials of degree $2N-1$, see [14].

5.2. **Two-dimensional expansions.** Consider $[-1, 1]^2 \subset \mathbb{R}^2$. We will use tensor products of nodal and edge functions to construct conforming finite dimensional subspaces $\mathbf{C}^h$, $\mathbf{D}^h$, $\mathbf{D}_0^h$ and S^h of $H(curl, \Omega)$, $H(div, \Omega)$, $\mathcal{D}$ and $L^2(\Omega)$, respectively. Let (ξ_i, η_j) be the GLL points in ξ- and η-direction. We will first describe the finite dimensional spaces and the primal vector operations, $\nabla\times$ and $\nabla\cdot$, between these space.

5.2.1. *Spaces and primal vector operators.* We define the curl-conforming space $\mathbf{C}^h$ as the span of the basis set $\{c_{ij}(\xi, \eta)\}$, $i, j = 0, \dots, N$, where $c_{ij}(\xi, \eta) = h_i(\xi) h_j(\eta)$. Thus an element $\boldsymbol{\omega}^h(\xi, \eta) \in \mathbf{C}^h$ of this space has the form

$$\boldsymbol{\omega}^h(\xi, \eta) = \sum_{i=0}^{N} \sum_{j=0}^{N} \omega_{i,j} c_{ij}(\xi, \eta) = [c_{00}(\xi, \eta) \ \dots \ c_{NN}(\xi, \eta)] \begin{bmatrix} \omega_{0,0} \\ \vdots \\ \omega_{N,N} \end{bmatrix} . \tag{44}$$

From (35) it follows that $\omega_{i,j} = \boldsymbol{\omega}(\xi_i, \eta_j)$. We will use the compact notation $\vec{\omega} = [\omega_{0,0}, \ldots, \omega_{N,N}]^T$ to denote the coefficient vector of $\boldsymbol{\omega}^h$. Taking the curl of $\boldsymbol{\omega}^h$ we obtain, using (41)

$$\nabla \times \boldsymbol{\omega}^h = \begin{pmatrix} \sum_{i=0}^{N} \sum_{j=1}^{N} (\omega_{i,j} - \omega_{i,j-1}) d_{ij}(\xi, \eta) \\ \sum_{i=1}^{N} \sum_{j=0}^{N} (\omega_{i-1,j} - \omega_{i,j}) d_{ji}(\eta, \xi) \end{pmatrix}$$

$$= \begin{bmatrix} d_{01}(\xi,\eta) & \ldots & d_{NN}(\xi,\eta) & 0 & \ldots & 0 \\ 0 & \ldots & 0 & d_{01}(\eta,\xi) & \ldots & d_{NN}(\eta,\xi) \end{bmatrix} \mathbb{E}^{1,0} \begin{bmatrix} \omega_{0,0} \\ \vdots \\ \omega_{N,N} \end{bmatrix}. \tag{45}$$

where $d_{ij}(\xi, \eta) = h_i(\xi) e_j(\eta)$, $d_{ij}(\eta, \xi) = h_i(\eta) e_j(\xi)$ and $\mathbb{E}^{1,0}$ is an *incidence matrix* containing the values -1, 0 and 1. This incidence matrix is very sparse.

We define the div-conforming space $\mathbf{D}^h$ as the span of $\{d_{ij}(\xi, \eta)\} \times \{d_{lk}(\eta, \xi\}$, for $i, l = 0, \ldots, N$ and $j, k = 1, \ldots, N$. The identity (45) shows that $\nabla\times : \mathbf{C}^h \to \mathbf{D}^h$. An element $\boldsymbol{f}^h \in \mathbf{D}^h$, has the form

$$\boldsymbol{f}^h(\xi, \eta) = \begin{pmatrix} \sum_{i=0}^{N} \sum_{j=1}^{N} f^{\xi}_{i,j} d_{ij}(\xi, \eta) \\ \sum_{i=1}^{N} \sum_{j=0}^{N} f^{\eta}_{i,j} d_{ji}(\eta, \xi) \end{pmatrix}$$

$$= \begin{bmatrix} d_{01}(\xi,\eta) & \ldots & d_{NN}(\xi,\eta) & 0 & \cdots & 0 \\ 0 & \ldots & 0 & d_{01}(\eta,\xi) & \ldots & d_{NN}(\eta,\xi) \end{bmatrix} \begin{bmatrix} f^{\xi}_{0,1} \\ \vdots \\ f^{\xi}_{N,N} \\ f^{\eta}_{1,0} \\ \vdots \\ f^{\eta}_{N,N} \end{bmatrix}. \tag{46}$$

Subsequently we will use the notation $\vec{f} = [f^{\xi}_{0,1}, \ldots, f^{\xi}_{N,N}, f^{\eta}_{1,0}, \ldots, f^{\eta}_{N,N}]^T$ for the coefficient vector of a function $\boldsymbol{f}^h \in \mathbf{D}^h$.

Since both $\nabla \times \boldsymbol{\omega}^h \in \mathbf{D}^h$ and $\boldsymbol{f}^h \in \mathbf{D}^h$, the equation $\nabla \times \boldsymbol{\omega}^h = \boldsymbol{f}^h$ is dimensionally consistent. After equating (45) and (46), we see that $\nabla \times \boldsymbol{\omega}^h = \boldsymbol{f}^h$ is equivalent to a linear system

$$\mathbb{E}^{1,0} \begin{bmatrix} \omega_{0,0} \\ \vdots \\ \omega_{N,N} \end{bmatrix} = \begin{bmatrix} f^{\xi}_{0,1} \\ \vdots \\ f^{\xi}_{N,N} \\ f^{\eta}_{1,0} \\ \vdots \\ f^{\eta}_{N,N} \end{bmatrix}, \tag{47}$$

that involves the topological incidence matrix but not the basis functions. The sparse incidence matrix $\mathbb{E}^{1,0}$ thus gives the purely topological part of $\nabla\times$, i.e., the part of this operator that remains the same so long as the mesh connectivity does not change. All metric properties, size and shape of the grid and the order of the scheme, are contained in the basis functions.

The space $\mathbf{D}_0^h$ is obtained from $\mathbf{D}^h$ by setting all fluxes over the outer boundary to zero. An element $\boldsymbol{u}^h \in \mathbf{D}_0^h$ is therefore represented as

$$\begin{aligned} \boldsymbol{u}^h(\xi,\eta) &= \begin{pmatrix} \sum_{i=1}^{N-1}\sum_{j=1}^{N} u^{\xi}_{i,j} d_{ij}(\xi,\eta) \\ \sum_{i=1}^{N}\sum_{j=1}^{N-1} u^{\eta}_{i,j} d_{ji}(\eta,\xi) \end{pmatrix} \\ &= \begin{bmatrix} d_{11}(\xi,\eta) & \dots & d_{N-1N}(\xi,\eta) & 0 & \dots & 0 \\ 0 & \dots & 0 & d_{11}(\eta,\xi) & \dots & d_{N-1,N}(\eta,\xi) \end{bmatrix} \begin{bmatrix} u^{\xi}_{1,1} \\ \vdots \\ u^{\xi}_{N-1,N} \\ u^{\eta}_{1,1} \\ \vdots \\ u^{\eta}_{N,N-1} \end{bmatrix} . \end{aligned} \tag{48}$$

For $\boldsymbol{u}^h \in \mathbf{D}_0^h$ the expansion of $\nabla \cdot \boldsymbol{u}^h$ is given by

$$\begin{aligned} \nabla \cdot \boldsymbol{u}^h &= \sum_{i=1}^{N}\sum_{j=1}^{N} \left(u^{\xi}_{i,j} - u^{\xi}_{i-1,j} + u^{\eta}_{i,j} - u^{\eta}_{i,j-1} \right) s_{ij}(\xi,\eta) \\ &= \begin{bmatrix} s_{11}(\xi,\eta) & \dots & s_{NN}(\xi,\eta) \end{bmatrix} \mathbb{E}^{2,1} \begin{bmatrix} u^{\xi}_{1,1} \\ \vdots \\ u^{\xi}_{N-1,N} \\ u^{\eta}_{1,1} \\ \vdots \\ u^{\eta}_{N,N-1} \end{bmatrix} , \end{aligned} \tag{49}$$

where $s_{ij}(\xi,\eta) = e_i(\xi) e_j(\eta)$, $u^{\xi}_{0,j} = u^{\xi}_{N,j} = u^{\eta}_{i,0} = u^{\eta}_{i,N} = 0$ in the first equality, and we have used (41). The incidence matrix $\mathbb{E}^{2,1}$ is a sparse matrix which only contains -1, 0 and 1. Similar to $\mathbb{E}^{1,0}$, this matrix gives the topological part of the divergence operator. As a result, the conservation of mass statement, $\nabla \cdot \boldsymbol{u}^h = 0$, reduces to the following relation for the expansion coefficients of $\boldsymbol{u}^h$

$$\mathbb{E}^{2,1} \begin{bmatrix} u^{\xi}_{1,1} \\ \vdots \\ u^{\xi}_{N-1,N} \\ u^{\eta}_{1,1} \\ \vdots \\ u^{\eta}_{N,N-1} \end{bmatrix} = 0 . \tag{50}$$

Finally, we define S^h to be the span of $\{s_{ij}(\xi,\eta)\}$ for $i, j = 1, \dots, N$. This space equals the range of the discrete divergence acting on $\mathbf{D}_0^h$, i.e., $\nabla \cdot \mathbf{D}_0^h = S^h$. Consequently, we use S^h to approximate the space $L^2(\Omega)$. The functions in S^h have the form

$$p^h(\xi,\eta) = \sum_{i=1}^{N}\sum_{j=1}^{N} p_{i,j} s_{ij}(\xi,\eta) . \tag{51}$$

We now have the conforming finite dimensional function spaces $\mathbf{C}^h \subset H(curl,\Omega)$, $\mathbf{D}^h \subset H(div,\Omega)$, $S^h \in L^2(\Omega)$, and $\mathbf{D}_0^h \subset \mathcal{D}$, such that $\mathbf{C}^h \xrightarrow{\nabla\times} \mathbf{D}^h \xrightarrow{\nabla\cdot} S^h$ forms an exact sequence.

5.3. **Inner products.** In this section we derive the algebraic representations of the inner products acting on the discrete spaces introduced earlier. These representations are also required to obtain the algebraic representations of the adjoint operators from Definition 1.

5.3.1. *Inner-product on* $\mathbf{C}^h$. Let $\boldsymbol{\xi}^h, \boldsymbol{\omega} \in \mathbf{C}^h$, then the L^2-inner product in $\mathbf{C}^h$ is given by

$$\left(\boldsymbol{\xi}^h, \boldsymbol{\omega}^h\right)_0 = \int_{-1}^{1}\int_{-1}^{1} \boldsymbol{\xi}^h \boldsymbol{\omega}^h \,\mathrm{d}\xi\mathrm{d}\eta = \vec{\xi}^T \mathbb{M}_C \vec{\omega} \,, \tag{52}$$

where $\mathbb{M}_C$ is the $(N+1)^2 \times (N+1)^2$ Gramm matrix of the basis $\{c_{ij}(\xi,\eta)\}$.

If we evaluate the integrals in this mass matrix using GLL integration, (42), and use (35), we see that $\mathbb{M}_C$ is a diagonal matrix with the product of the integration weights (43) on the diagonal.

5.3.2. *Inner-product on* $\mathbf{D}^h$. For $\boldsymbol{u}^h, \boldsymbol{v}^h \in \mathbf{D}^h$ the inner-product is given by

$$\left(\boldsymbol{u}^h, \boldsymbol{v}^h\right)_0 = \int_{-1}^{1}\int_{-1}^{1} (\boldsymbol{u}^h, \boldsymbol{v}^h) \,\mathrm{d}\xi\mathrm{d}\eta = \vec{v}^T \mathbb{M}_D \vec{u} \,. \tag{53}$$

Here the matrix $\mathbb{M}_D$ corresponds to the Gramm matrix of the basis functions $\{d_{ij}\} \times \{d_{kl}\}$. This matrix is a $2N(N+1) \times 2N(N+1)$ block diagonal matrix, but it is not diagonal.

5.3.3. *Inner-product on* $\mathbf{D}^h_0$. The mass matrix $\mathbb{M}_{D_0}$ on $\mathbf{D}^h_0$ is obtained from $\mathbb{M}_D$ by removing the row and columns which correspond to the prescribed zero fluxes on the boundary. $\mathbb{M}_{D_0}$ is then a $2N(N-1) \times 2N(N-1)$ block diagonal matrix.

5.3.4. *Inner product in weak* L^2*-norm.* In the weak L^2-norm $\|\cdot\|_{\mathcal{D}}$ we project the degrees of freedom of $\vec{f} \in \mathbf{D}^h$ onto the degrees of freedom in $\mathbf{D}^h_0$. So we look for vector of degrees of freedom $\vec{u}_f \in \mathbf{D}^h_0$ such that

$$\vec{v}^T \mathbb{M}_{D_0} \vec{u}_f = \vec{v}^T \mathbb{M}_{D_0 D} \vec{f} \,.$$

The mass matrix $\mathbb{M}_{D_0 D}$ is obtained from $\mathbb{M}_D$ by eliminating the rows which correspond to the prescribed zero fluxes in $\mathbf{D}_0$. The matrix $\mathbb{M}_{D_0 D}$ is non-square. The degrees of freedom for the projected degrees of freedom $\vec{u}_f$ are then given by

$$\vec{u}_f = \mathbb{M}^{-1}_{D_0} \mathbb{M}_{D_0 D} \vec{f} \,.$$

In particular, we have that the projection of the degrees of freedom of $\nabla \times \boldsymbol{\omega}^h$ on $\mathbf{D}_0$ is given by

$$\mathbb{M}^{-1}_{D_0} \mathbb{M}_{D_0 D} \mathbb{E}^{(1,0)} \vec{\omega} \,. \tag{54}$$

5.3.5. *Inner-product on* S^h. The mass matrix $\mathbb{M}_S$ for S^h corresponds to the Gramm matrix of the basis $s_{ij}(\xi,\eta)$, $i,j = 1,\ldots,N$ given in (51). The mass matrix $\mathbb{M}_S$ is not diagonal, but diagonal dominant.

5.4. **Finite dimensional adjoint operators.** Using the algebraic expressions for the primary operators $\nabla\times$ and $\nabla\cdot$ in terms of the incidence matrices given in Section 5.2.1, and the algebraic forms of the inner products in Section 5.3, we can easily obtain the algebraic forms of the adjoint operators in Definition 1.

Let $\boldsymbol{\xi}^h \in \mathbf{C}^h$, then $\nabla \times \boldsymbol{\xi}^h \in \mathbf{D}^h$, if we take the inner-product with any $\boldsymbol{v}^h \in \mathbf{D}^h_0$ we have in terms of the expansion coefficients of $\vec{\xi}$ and $\vec{v}$

$$\begin{aligned} \left(\boldsymbol{v}^h, \nabla \times \boldsymbol{\xi}^h\right)_0 &= \vec{v}^T \mathbb{M}_{D_0 D} \mathbb{E}^{1,0} \vec{\xi} = \vec{v}^T \mathbb{M}_{D_0 D} \mathbb{E}^{1,0} \mathbb{M}_C^{-1} \mathbb{M}_C \vec{\xi} \\ &= (\mathbb{M}_C^{-1} \mathbb{E}^{1,0^T} \mathbb{M}^T_{D_0 D} \vec{v})^T \mathbb{M}_C \vec{\xi} = \left(\nabla^* \times \boldsymbol{v}^h, \boldsymbol{\xi}^h\right)_0 \,, \end{aligned} \tag{55}$$

where we used the fact that the tangential velocity of $\boldsymbol{v}^h$ is zero for $\boldsymbol{v} \in \mathbf{D}_0^h \subset \mathcal{D}$. It follows that the algebraic form of $\nabla^* \times \boldsymbol{v}^h$ is given by

$$\mathbb{M}_C^{-1}\mathbb{E}^{1,0^T}\mathbb{M}_{D_0D}^T\vec{v}\,. \tag{56}$$

Let $\boldsymbol{v}^h \in \mathbf{D}_0^h$ then $\nabla \cdot \boldsymbol{v}^h \in S^h$. If we take the inner-product with any $p \in S^h$, we obtain in terms of the expansion coefficients of $\vec{v}$ and $\vec{p}$

$$\begin{aligned}(p^h, \nabla \cdot \boldsymbol{v}^h)_0 &= \vec{p}^T\mathbb{M}_S\mathbb{E}^{2,1}\vec{v} = \vec{p}^T\mathbb{M}_S\mathbb{E}^{2,1}\mathbb{M}_{D_0}^{-1}\mathbb{M}_{D_0}\vec{v} \\ &= (\mathbb{M}_{D_0}^{-1}\mathbb{E}^{2,1^T}\mathbb{M}_S\vec{p})^T\mathbb{M}_{D_0}\vec{v} = (-\nabla^* p^h, \boldsymbol{v}^h)_0\,,\end{aligned} \tag{57}$$

where again the boundary integral vanishes for $\boldsymbol{v}^h \in \mathbf{D}_0^h \subset \mathcal{D}$. Therefore, the algebraic form of $\nabla^* p^h \in \mathbf{D}_0^h$ is given by

$$-\mathbb{M}_{D_0}^{-1}\mathbb{E}^{2,1^T}\mathbb{M}_S\vec{p}\,. \tag{58}$$

5.5. **Mimetic least-squares for the Stokes problem.** With the conforming finite dimensional spaces and the primary and adjoint vector operations between these spaces, we are now in the position to implement (34).

Using the algebraic forms of the inner products and operators derived in the previous subsections it is not difficult to see that the discrete Euler-Lagrange equation (34) is equivalent to a linear algebraic system

$$\mathbb{S}\vec{x} = rhs\,, \tag{59}$$

where $\mathbb{S}$ is 3×3 block matrix given by

(60)
$$\begin{pmatrix} \mathbb{E}^{1,0^T}\mathbb{M}_{D_0D}^T\mathbb{M}_{D_0}^{-1}\mathbb{M}_{D_0D}\mathbb{E}^{1,0} + \mathbb{M}_C & -\mathbb{E}^{1,0^T}\mathbb{M}_{D_0D}^T & -\mathbb{E}^{1,0^T}\mathbb{M}_{D_0D}^T\mathbb{M}_{D_0}^{-1}\mathbb{E}^{2,1^T}\mathbb{M}_S \\ -\mathbb{M}_{D_0D}\mathbb{E}^{1,0} & \mathbb{M}_{D_0D}\mathbb{E}^{1,0}\mathbb{M}_C^{-1}\mathbb{E}^{1,0^T}\mathbb{M}_{D_0D}^T + \mathbb{E}^{2,1^T}\mathbb{M}_S\mathbb{E}^{2,1} & 0 \\ -\mathbb{M}_S\mathbb{E}^{2,1}\mathbb{M}_{D_0}^{-1}\mathbb{M}_{D_0D}\mathbb{E}^{1,0} & 0 & \mathbb{M}_S\mathbb{E}^{2,1}\mathbb{M}_{D_0}^{-1}\mathbb{E}^{2,1^T}\mathbb{M}_S \end{pmatrix},$$

$$\vec{x} = \begin{pmatrix} \vec{\omega} \\ \vec{u} \\ \vec{p} \end{pmatrix},$$

and

$$rhs = \begin{pmatrix} \mathbb{E}^{1,0^T}\mathbb{M}_{D_0D}^T\mathbb{M}_{D_0}^{-1}\mathbb{M}_{D_0D}\vec{f} \\ 0 \\ -\mathbb{M}_S\mathbb{E}^{2,1}\mathbb{M}_{D_0}^{-1}\mathbb{M}_{D_0D}\vec{f} \end{pmatrix}.$$

We see that this discrete system involves only mass matrices and incidence matrices related to the various spaces and operations between these spaces. We started this section by stating that a mimetic method aims to decompose a PDE in a purely topological part and a metric dependent part. The mimetic least-squares formulation precisely achieves this, where the topological part is represented by the incidence matrices and the metric dependent part by the mass matrices.

The discrete least-squares system matrix (59) can be factorized as

$$\mathbb{A}^T\mathbb{M}\mathbb{A}\vec{x} = \mathbb{A}^T\mathbb{M}\vec{b}\,,$$

where

$$\mathbb{A} = \begin{pmatrix} \mathbb{I} & -\mathbb{M}_C^{-1}\mathbb{E}^{1,0^T}\mathbb{M}_{D_0D}^T & 0 \\ \mathbb{M}_{D_0}^{-1}\mathbb{M}_{D_0D}\mathbb{E}^{1,0} & 0 & -\mathbb{M}_{D_0}^{-1}\mathbb{E}^{2,1^T}\mathbb{M}_S \\ 0 & \mathbb{E}^{2,1} & 0 \end{pmatrix},$$

and

$$\mathbb{M} = \begin{pmatrix} \mathbb{M}_C & 0 & 0 \\ 0 & \mathbb{M}_{D_0} & 0 \\ 0 & 0 & \mathbb{M}_S \end{pmatrix} \quad \text{and} \quad \vec{b} = \begin{pmatrix} 0 \\ \mathbb{M}_{D_0}^{-1}\mathbb{M}_{D_0 D}\vec{f} \\ 0 \end{pmatrix}.$$

Note that the matrix $\mathbb{A}$ contains all the operations we introduced in this section: In the first row we see the operator $\mathbb{M}_C^{-1}\mathbb{E}^{1,0^T}\mathbb{M}_{D_0 D}^T$ which by (56) is the discrete $\nabla^*\times$. In the second row we have $\mathbb{M}_{D_0}^{-1}\mathbb{M}_{D_0 D}\mathbb{E}^{1,0}$ which by (54) is the projection of $\nabla\times\boldsymbol{\omega}^h$ onto $\mathbf{D}_0$. The operator $-\mathbb{M}_{D_0}^{-1}\mathbb{E}^{2,1^T}\mathbb{M}_S$ is by (58) the discrete ∇^* and in the last row we have $\mathbb{E}^{2,1}$ which by (50) is the discrete divergence operator $\nabla\cdot$ acting on $\mathbf{D}_0$.

If $\vec{x}$ is a solution of the system $\mathbb{A}\vec{x} = \vec{b}$, then $\vec{x}$ is also a solution of (59) and by the uniqueness of the least-squares formulation it is the only solution of (59). Note that the system $\mathbb{M}\mathbb{A}\vec{x} = \mathbb{M}\vec{b}$ was solved in [23].

Theorem 3. *The solution of the least-squares formulation* (59) *is locally mass conserving.*

Proof. If $\vec{x}$ is a solution of (59) then it also solves $\mathbb{A}\vec{x} = \vec{b}$. In particular, this means that $\mathbb{E}^{2,1}\vec{u} = 0$. But according to (49) and (50) this equation is precisely the algebraic equivalent of $\nabla\cdot\boldsymbol{u}^h = 0$, i.e., the velocity solution of the least-squares method (34) is exactly divergence-free. □

Theorem 4. *Let $\boldsymbol{\omega}^h$ be the solution of the least-squares formulation* (59)*, then*

$$\int_\Omega \boldsymbol{\omega}^h \,\mathrm{d}\Omega = 0\,.$$

Proof. In 2D at the continuous level we have that $\boldsymbol{\omega} = \nabla\times\boldsymbol{u}$ implies that

$$\int_\Omega \boldsymbol{\omega}\,\mathrm{d}\Omega = \int_\Omega \nabla\times\boldsymbol{u}\,\mathrm{d}\Omega = \int_{\partial\Omega} \boldsymbol{u}\times\boldsymbol{n}\,\mathrm{d}S = 0\,,$$

if $\boldsymbol{u}\times\boldsymbol{n} = 0$ along the boundary. In the finite dimensional case, the same result follows by taking for $\boldsymbol{\xi}^h$ the constant function $\boldsymbol{\xi}^h = 1$ in (34) and $\boldsymbol{v}^h = 0$ and $q^h = 0$. Then the least-squares formulation reduces to

$$(1, \boldsymbol{\omega}^h)_0 = \int_\Omega 1\cdot\boldsymbol{\omega}^h \mathrm{d}S = 0\,.$$

Or, in terms of (59),

$$(1,\ldots,1)\mathbb{M}_C \begin{pmatrix} \omega_{0,0} \\ \vdots \\ \omega_{N,N} \end{pmatrix} = \sum_{i=0}^{N}\sum_{j=0}^{N} \omega_{i,j} w_i w_j = 0\,, \tag{61}$$

because by Section 5.3.1 $\mathbb{M}_C$ is a diagonal matrix which contains the products of the GLL-integration weights (43) on its diagonal. Therefore (61) shows that the numerical integral of $\boldsymbol{\omega}^h$ over the domain is zero, where $\boldsymbol{\omega}^h$ is a polynomial of degree N in the ξ- and η-direction. Since GLL-integration is exact for polynomials up to $2N-1$, (61) implies that

$$\int_\Omega \boldsymbol{\omega}^h \,\mathrm{d}\Omega = 0\,.$$

□

6. Numerical results

In this section we use several manufactured solution examples to asses the performance of the spectral mimetic least-squares method.

6.1. **Test case 1.** Consider the Stokes problem defined on the domain $\Omega = [-1, 1]^2$ with $\boldsymbol{u} = 0$ along the boundary. We take as exact divergence-free velocity field

(62)
$$\boldsymbol{u}(x, y) = \begin{pmatrix} -4y(1-y^2)(1-x^2)^2 \sin(2\pi(x+y)) + 2\pi(1-x^2)^2(1-y^2)^2 \cos(2\pi(x+y)) \\ 4x(1-x^2)(1-y^2)^2 \sin(2\pi(x+y)) - 2\pi(1-x^2)^2(1-y^2)^2 \cos(2\pi(x+y)) \end{pmatrix}.$$

For the right hand side function $\boldsymbol{f}$ we take $\boldsymbol{f} = \nabla \times \nabla^* \times \boldsymbol{u}$. In this case the corresponding exact pressure field is constant. The problem is solved on one spectral element with varying polynomial degree N. For such a small problem system (59) can be solved with a direct solver, where we used direct inverses of the mass matrices which appear in the system.

N	4	6	8	10	12	14	16	18
$\mathcal{J}(\omega^h, \boldsymbol{u}^h, p^h; \boldsymbol{f})$	$1.6 \cdot 10^{5}$	$1.5 \cdot 10^{5}$	$4.8 \cdot 10^{4}$	$4.0 \cdot 10^{3}$	$1.0 \cdot 10^{2}$	$1.1 \cdot 10^{0}$	$5.7 \cdot 10^{-3}$	$1.6 \cdot 10^{-5}$
$\frac{1}{2}\|\omega^h - \nabla^* \times \boldsymbol{u}^h\|_0^2$	$3.6 \cdot 10^{-26}$	$9.1 \cdot 10^{-27}$	$1.1 \cdot 10^{-25}$	$4.1 \cdot 10^{-25}$	$3.1 \cdot 10^{-25}$	$5.0 \cdot 10^{-25}$	$9.8 \cdot 10^{-25}$	$1.2 \cdot 10^{--24}$
$\frac{1}{2}\|\nabla \times \omega^h + \nabla^* p - f\|_{\mathcal{D}}^2$	$1.6 \cdot 10^{5}$	$1.5 \cdot 10^{5}$	$4.8 \cdot 10^{4}$	$4.0 \cdot 10^{3}$	$1.0 \cdot 10^{2}$	$1.1 \cdot 10^{0}$	$5.7 \cdot 10^{-3}$	$1.6 \cdot 10^{-5}$
$\frac{1}{2}\|\nabla \cdot \boldsymbol{u}^h\|_0^2$	$6.6 \cdot 10^{-26}$	$1.4 \cdot 10^{-26}$	$1.4 \cdot 10^{-25}$	$3.1 \cdot 10^{-25}$	$3.7 \cdot 10^{-25}$	$5.7 \cdot 10^{-25}$	$1.2 \cdot 10^{-24}$	$1.3 \cdot 10^{-24}$
$\|\omega^h - \omega\|_C^2$	$3.3 \cdot 10^{5}$	$3.1 \cdot 10^{5}$	$9.6 \cdot 10^{4}$	$8.0 \cdot 10^{3}$	$2.1 \cdot 10^{2}$	$2.2 \cdot 10^{0}$	$1.1 \cdot 10^{-2}$	$3.2 \cdot 10^{-5}$
$\|\boldsymbol{u}^h - \boldsymbol{u}\|_{div}^2$	$5.1 \cdot 10^{1}$	$3.5 \cdot 10^{1}$	$7.4 \cdot 10^{0}$	$6.3 \cdot 10^{-1}$	$1.7 \cdot 10^{-2}$	$1.9 \cdot 10^{-4}$	$1.0 \cdot 10^{-6}$	$3.0 \cdot 10^{-9}$
$\|p^h - p\|_{\mathcal{D}}^2$	$1.0 \cdot 10^{4}$	$8.1 \cdot 10^{2}$	$9.7 \cdot 10^{0}$	$7.8 \cdot 10^{-1}$	$1.1 \cdot 10^{-2}$	$6.6 \cdot 10^{-4}$	$1.8 \cdot 10^{-7}$	$2.6 \cdot 10^{-10}$

TABLE 1. Convergence results for Test case 1 with increasing polynomial degree

The first four rows in Table 1 show the value of the least-squares functional and the residuals that make it up for increasing polynomial degree N. The last three rows give the errors in the vorticity, velocity and the pressure, measured in $\|\cdot\|_C^2$, $\|\cdot\|_{div}$, and $\|\cdot\|_{\mathcal{D}}^2$-norm, respectively.

The first thing to note is that conservation of mass is satisfied up to machine precision for all polynomial degrees. This result confirms Theorem 3.

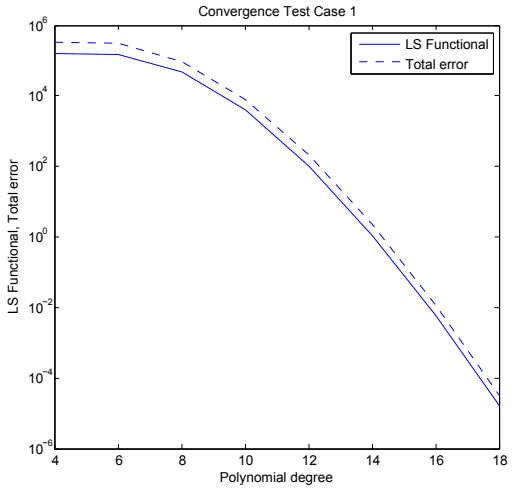

FIGURE 1. Convergence of the least-squares functional $\mathcal{J}$ and the total error $\|\omega^h - \omega\|_C^2 + \|\boldsymbol{u}^h - \boldsymbol{u}\|_{div}^2 + \|p^h - p\|_{\mathcal{D}}^2$ as a functional of the polynomial degree N for Test case 1.

Test case 1 shows that the least-squares functional is dominated by the residual of the momentum equation. In the total error the weak $H(curl, \Omega)$-norm of the vorticity dominates the total error. The ratio of the least-squares functional value over total error is approximately 0.5.

For a well-posed least-squares formulation the convergence rate of the least-squares functional should be equal to the convergence rate of the total error. In Figure 1 the convergence of the least-squares functional and the total error are plotted as a function of the polynomial degree N and both quantities converge at the same (exponential) rate.

6.2. **Test case 2.** Consider the Stokes problem defined on the domain $\Omega = [-1, 1]^2$ with $\boldsymbol{u} = 0$ along the boundary. The right hand side function $\boldsymbol{f}$ in this case is given by

$$f(x, y) = \begin{pmatrix} \pi \cos(\pi(x + y)) \\ \pi \cos(\pi(x + y)) \end{pmatrix} . \tag{63}$$

This particular flow corresponds to a pressure field given by

$$p(x, y) = \sin(\pi(x + y)) + C \ , \tag{64}$$

where C is an arbitrary constant. The velocity and vorticity for this problem are identically zero.

N	4	6	8	10	12	14	16	18
$\mathcal{J}(\omega^h, \boldsymbol{u}^h, p^h; \boldsymbol{f})$	$8.1 \cdot 10^{0}$	$1.8 \cdot 10^{-1}$	$8.5 \cdot 10^{-4}$	$1.2 \cdot 10^{-6}$	$6.0 \cdot 10^{-10}$	$1.8 \cdot 10^{-13}$	$2.9 \cdot 10^{-17}$	$6.0 \cdot 10^{-17}$
$\frac{1}{2}\|\omega^h - \nabla^* \times \boldsymbol{u}^h\|_0^2$	$8.4 \cdot 10^{-29}$	$4.5 \cdot 10^{-27}$	$1.0 \cdot 10^{-25}$	$4.1 \cdot 10^{-24}$	$1.4 \cdot 10^{-22}$	$4.2 \cdot 10^{-22}$	$5.6 \cdot 10^{-22}$	$7.1 \cdot 10^{-21}$
$\frac{1}{2}\|\nabla \times \omega^h + \nabla^* p - f\|_D^2$	$8.1 \cdot 10^{0}$	$1.8 \cdot 10^{-1}$	$8.5 \cdot 10^{-4}$	$1.2 \cdot 10^{-6}$	$6.9 \cdot 10^{-10}$	$1.8 \cdot 10^{-13}$	$2.9 \cdot 10^{-17}$	$6.0 \cdot 10^{-17}$
$\frac{1}{2}\|\nabla \cdot \boldsymbol{u}^h\|_0^2$	$1.2 \cdot 10^{-28}$	$8.9 \cdot 10^{-27}$	$1.3 \cdot 10^{-25}$	$5.5 \cdot 10^{-24}$	$2.4 \cdot 10^{-22}$	$6.3 \cdot 10^{-22}$	$7.1 \cdot 10^{-22}$	$1.1 \cdot 10^{-20}$
$\|\omega^h - \omega\|_C^2$	$3.2 \cdot 10^{-26}$	$1.4 \cdot 10^{-23}$	$4.3 \cdot 10^{-22}$	$4.2 \cdot 10^{-20}$	$5.0 \cdot 10^{-18}$	$1.9 \cdot 10^{-17}$	$2.4 \cdot 10^{-17}$	$5.5 \cdot 10^{-16}$
$\|\boldsymbol{u}^h - \boldsymbol{u}\|_{div}^2$	$3.5 \cdot 10^{-29}$	$4.5 \cdot 10^{-28}$	$7.4 \cdot 10^{-27}$	$1.9 \cdot 10^{-25}$	$1.3 \cdot 10^{-24}$	$3.6 \cdot 10^{-24}$	$1.2 \cdot 10^{-23}$	$1.8 \cdot 10^{-22}$
$\|p^h - p\|_{\mathcal{D}}^2$	$1.6 \cdot 10^{1}$	$3.7 \cdot 10^{-1}$	$1.7 \cdot 10^{-3}$	$2.4 \cdot 10^{-6}$	$1.4 \cdot 10^{-9}$	$3.7 \cdot 10^{-13}$	$8.7 \cdot 10^{-17}$	$7.9 \cdot 10^{-16}$

TABLE 2. Convergence results for Test case 2 with increasing polynomial degree

The results for test case 2 are listed in Table 2. We see that for all polynomial degrees we can capture exactly the zero velocity and vorticity field (up to machine accuracy) and therefore also mass conservation is satisfied up to machine precision.

In Test case 2, the least-squares functional is again dominated by the residual of the momentum equation, while the total error in this case is dominated by the weak seminorm $\|p - p^h\|_{\mathcal{D}}$. The ratio of the least-squares functional over the total error is again approximately equal to 0.5 for all polynomial degrees.

For a well-posed least-squares formulation the least-squares functional converges at the same rate as the total error. In Figure 2 both the least-squares functional and the total error are plotted as a function of the polynomial degree and both quantities converge again at the same (exponential) rate until $N = 16$. For $N = 16$ all errors and residuals have reached zero machine accuracy, $O(10^{-17})$. Beyond $N = 16$ the truncation error becomes visible and the least-squares functional and the total error stall or start to increase slightly as can be seen in Figure 2.

6.3. **Test case 3.** In Test case 1 we used a divergence-free right hand side function, while in Test case 2 the right hand side function was irrotational. In this test case, we combine these two cases by using the exact velocity field from Test case 1 and the exact pressure field from Test case 2. The corresponding right hand side function is then given by

$$\boldsymbol{f} = \nabla \times \nabla^* \times \boldsymbol{u} + \nabla^* p \ . \tag{65}$$

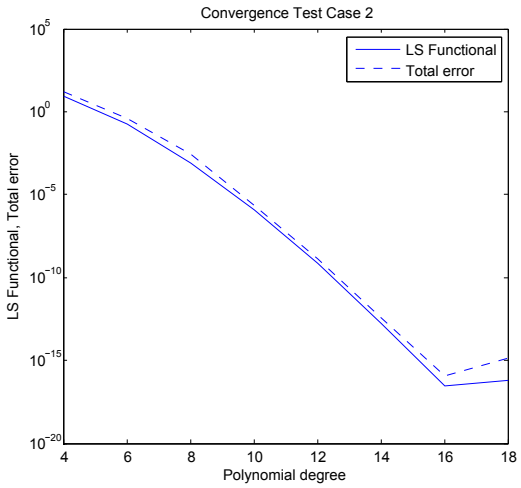

FIGURE 2. Convergence of the least-squares functional $\mathcal{J}$ and the total error $\|\omega^h-\omega\|_C^2+\|\boldsymbol{u}^h-\boldsymbol{u}\|_{div}^2+\|p^h-p\|_{\mathcal{D}}^2$ as a functional of the polynomial degree N for Test case 2.

The results of this test case are displayed in Table 3

N	4	6	8	10	12	14	16	18
$\mathcal{J}(\omega^h,\boldsymbol{u}^h,p^h;\boldsymbol{f})$	$1.6\cdot10^{5}$	$1.5\cdot10^{5}$	$4.8\cdot10^{4}$	$4.0\cdot10^{3}$	$1.0\cdot10^{2}$	$1.1\cdot10^{0}$	$5.7\cdot10^{-3}$	$1.6\cdot10^{-5}$
$\frac{1}{2}\|\omega^h-\nabla^*\times\boldsymbol{u}^h\|_0^2$	$3.7\cdot10^{-26}$	$1.1\cdot10^{-26}$	$4.7\cdot10^{-25}$	$3.1\cdot10^{-24}$	$2.1\cdot10^{-22}$	$8.4\cdot10^{-21}$	$1.2\cdot10^{-21}$	$9.0\cdot10^{-21}$
$\frac{1}{2}\|\nabla\times\omega^h+\nabla^* p-f\|_D^2$	$1.6\cdot10^{5}$	$1.5\cdot10^{5}$	$4.8\cdot10^{4}$	$4.0\cdot10^{3}$	$1.0\cdot10^{2}$	$1.1\cdot10^{0}$	$5.7\cdot10^{-3}$	$1.6\cdot10^{-5}$
$\frac{1}{2}\|\nabla\cdot\boldsymbol{u}^h\|_0^2$	$6.2\cdot10^{-26}$	$1.8\cdot10^{-26}$	$4.6\cdot10^{-25}$	$4.9\cdot10^{-24}$	$4.0\cdot10^{-22}$	$1.3\cdot10^{-22}$	$1.5\cdot10^{-21}$	$5.9\cdot10^{-21}$
$\|\omega^h-\omega\|_C^2$	$3.3\cdot10^{5}$	$3.1\cdot10^{5}$	$9.6\cdot10^{4}$	$8.0\cdot10^{3}$	$2.1\cdot10^{2}$	$2.2\cdot10^{0}$	$1.1\cdot10^{-2}$	$3.2\cdot10^{-5}$
$\|\boldsymbol{u}^h-\boldsymbol{u}\|_{div}^2$	$5.1\cdot10^{1}$	$3.5\cdot10^{1}$	$7.3\cdot10^{0}$	$6.3\cdot10^{-1}$	$1.7\cdot10^{-2}$	$1.9\cdot10^{-4}$	$1.0\cdot10^{-6}$	$3.0\cdot10^{-9}$
$\|p^h-p\|_{\mathcal{D}}^2$	$1.0\cdot10^{4}$	$8.2\cdot10^{1}$	$9.7\cdot10^{0}$	$7.8\cdot10^{-1}$	$1.1\cdot10^{-2}$	$6.6\cdot10^{-5}$	$1.8\cdot10^{-7}$	$2.6\cdot10^{-10}$

TABLE 3. Convergence results for Test case 3 with increasing polynomial degree

The convergence results for Test case 3 are very similar to those of Test case 1. While all residuals go to zero with increasing polynomial degree, conservation of mass, $\nabla\cdot\boldsymbol{u}^h=0$, is satisfied up to machine accuracy for all polynomial degrees.

In these 3 test cases the no-slip condition is enforced weakly without the need for adjustable parameters to enforce the no-slip constraint which is usually employed in least-squares finite element methods.

Theorem 4 predicts that the total integrated vorticity of the least-squares approximation will be zero. For all three test cases given above the total integrated vorticity is determined by GLL-integration and the results are listed in Table 4. That the integrated vorticity in Test case 2 is approximately equal to zero is not surprising because in this case the exact and numerical vorticity are zero. But for test cases 1 and 2 the vorticity in the domain ranges from -75 to $+75$. In all cases the integrated vorticity is zero up to machines precision, independent of the polynomial degree N, i.e. independent of how accurate the numerical approximation $\boldsymbol{\omega}^h$ is.

*Case**N*	4	6	8	10	12	14	16	18
1	$-2.8 \cdot 10^{-14}$	$6.0 \cdot 10^{-14}$	$6.8 \cdot 10^{-14}$	$-9.1 \cdot 10^{-13}$	$2.2 \cdot 10^{-13}$	$2.1 \cdot 10^{-13}$	$-1.1 \cdot 10^{-12}$	$3.0 \cdot 10^{-14}$
2	$5.4 \cdot 10^{-16}$	$-2.9 \cdot 10^{-16}$	$1.5 \cdot 10^{-14}$	$-1.2 \cdot 10^{-13}$	$1.0 \cdot 10^{-12}$	$-4.7 \cdot 10^{-13}$	$6.6 \cdot 10^{-12}$	$-1.3 \cdot 10^{-11}$
3	$-2.1 \cdot 10^{-13}$	$-3.7 \cdot 10^{-14}$	$-9.5 \cdot 10^{-13}$	$-5.4 \cdot 10^{-13}$	$9.1 \cdot 10^{-13}$	$-7.5 \cdot 10^{-13}$	$-1.7 \cdot 10^{-12}$	$-5.7 \cdot 10^{-12}$

TABLE 4. Integrated vorticity over the domain $\Omega = [-1, 1]^2$ for Test cases 1,2 & 3 for various polynomial degrees N.

7. Discussion

In this paper we developed a mimetic least-squares spectral element formulation for Stokes flow with no-slip (velocity) boundary conditions $\boldsymbol{u} = 0$ along the boundary of the domain. A crucial ingredient in the analysis is the Hodge-Morrey-Friedrichs decomposition of vector fields with $\boldsymbol{u} = 0$ along the boundary into a divergence-free part and an irrotational part which both satsify $\boldsymbol{u} = 0$ along the boundary.

A non-standard stability proof for well-posedness is required in order to bound the momentum equation in $H(div, \Omega)$ from below to establish well-posedness of the least-squares formulation.

Conforming finite dimensional function spaces have been constructed in a spectral element context as well as the primary and adjoint operators between these spaces.

All these operations can be represented by operations on the expansion coefficients, i.e. on the degrees of freedom in the various functions spaces. These operations can be divided in topological operations by means of incidence matrices and metric-dependent operations represented by mass matrices.

Although the no-slip condition is enforced weakly in the new formulation, this procedure does not involve any adjustable, mesh-dependent parameters.

We prove that for the mimetic least-squares formulation mass is exactly conserved. Numerical tests for non-trivial right-hand side functions confirms exact mass conservation for all polynomial degrees. Furthermore, we proved that the integrated vorticity of the least-squares solution $\boldsymbol{\omega}^h$ is equal to zero. This result is also confirmed by the test cases. The least-squares functional is dominated by the residual in the momentum equation. The residuals of mass conservation and the vorticity-velocity relation are zero up to machine accuracy.

Future work will focus on multi-element methods, curvilinear grids and error estimates based on the current least-squares formalism.

Acknowledgments

This material is based upon work supported by the U.S. Department of Energy, Office of Science, Office of Advanced Scientific Computing Research.

Our work had also been strongly influenced by the pioneering research of Max Gunzburger in least-squares finite element methods. Most notably, his work with G. Fix and N. Nicolaides on the grid decomposition property [19, 20] is among the earliest examples of the use of Hodge decomposition ideas in the analysis of finite element methods. These ideas have served as a catalysts for the authors to pursue investigation of compatible, mimetic least-squares finite element methods.

The authors also appreciate the thorough review of the paper by the anonymous referees. Their comments and suggestions helped to significantly improve our results and the presentation.

References

[1] D. Arnold, R. Falk, and R. Winther. Finite element exterior calculus, homological techniques, and applications. *Acta Numerica*, 15:1–155, 2006.

[2] H. Bhatia, G. Norgard, V. Pascussi, and P.-T. Bremer. The Helmholtz-Hodge Decomposition – A Survey. *IEEE Transactions on Visualization and Computer Graphics*, 19:1386–1404, 2013.

[3] P. Bochev and M. Gerritsma. A spectral mimetic least-squares method. *Computers and Mathematics with Applications*, 86:1480–1502, 2014.

[4] P. Bochev and M. Gunzburger. Analysis of least-squares finite element methods for the Stokes equations. *Math. Comp.*, 63:479–506, 1994.

[5] P. Bochev and M. Gunzburger. A locally conservative mimetic least-squares finite element method for the Stokes equations. In I. Lirkov, S. Margenov, and J. Wasniewski, editors, *In proceedings LSSC 2009*, volume 5910 of *Springer Lecture Notes in Computer Science*, pages 637–644, 2009.

[6] P. Bochev and M. Gunzburger. *Least-Squares finite element methods*, volume 166 of *Applied Mathematical Sciences*. Springer Verlag, 2009.

[7] P. Bochev and J. Hyman. Principles of mimetic disrcertizations of differential operators. In R. N. D. Arnold, P. Bochev and M. Shashkov, editors, *Compatible Spatial Discretizations*, volume 42 of *The IMA volumes in Mathematics and its Applications*, pages 89–119. Springer Verlag, 2006.

[8] P. Bochev, J. Lai, and L. Olson. A locally conservative, discontinuous least-squares finite element method for the Stokes equations. *International Journal for Numerical Methods in Fluids*, 68(6):782–804, 2012.

[9] P. Bochev, J. Lai, and L. Olson. A non-conforming least-squares finite element method for incompressible fluid flow problems. *International Journal for Numerical Methods in Fluids*, 72(3):375–402, 2013.

[10] P. B. Bochev. Negative norm least-squares methods for the velocity-vorticity-pressure Navier–Stokes equations. *Numerical Methods for Partial Differential Equations*, 15(2):237–256, 1999.

[11] J. Bonelle and A. Ern. Analysis of compatible discrete operator schemes for the Stokes equations on polyhedral meshes. *IMA Journal of Numerical Analysis*, to appear:1–26, 2014.

[12] A. Bossavit. On the geometry of electromagnetism. *Journal of the Japanese Society of Applied Electromagnetics and Mechanics*, 6:17–28 (no 1), 114–23 (no 2), 233–40 (no 3), 318–26 (no 4), 1998.

[13] A. Bossavit. Computational electromagnetism and geometry. *Journal of the Japanese Society of Applied Electromagnetics and Mechanics*, 7, 8:150–9 (no 1), 294–301 (no 2), 401–408 (no 3), 102–109 (no 4), 203–209 (no 5), 372–377 (no 6), 1999, 2000.

[14] C. Canuto, M. Hussaini, A. Quarteroni, and T. Zang. *Spectral Methods in Fluid Dynamics*. Springer-Verlag, 1987.

[15] C. Chang and J. Nelson. Least-squares finite element method for the Stokes problem with zero residual of mass conservation. *SIAM J. Numer. Anal.*, 34:480–489, 1997.

[16] J. Deang and M. Gunzburger. Issues related to least-squares finite element methods for the Stokes equations. *SIAM J. Sci. Comput.*, 20:878–906, 1998.

[17] L. Demkowicz. Polynomial exact sequences and projection-based interpolation with application to Maxwell equations. In D. Boffi, L. Demkowicz, R. Falk, F. Brezzi, R. Durán, and M. Fortin, editors, *Mixed Finite Elements, Compatibility Conditions, and Applications*, pages 101 – 158. Springer, 2008.

[18] M. Desbrun, A. Hirani, M. Leok, and J. Marsden. Discrete Exterior Calculus. *Arxiv preprint math/0508341*, 2005.
[19] G. Fix, M. Gunzburger, and R. Nicolaides. On mixed finite element methods for first order elliptic systems. *Numerische Mathematik*, 37(1):29–48, 1981.
[20] G. J. Fix, M. Gunzburger, and R. Nicolaides. On finite element methods of the least-squares type. *Comput. Math. Appl.*, 5:87–98, 1979.
[21] K. Friedrichs. Differential forms on Riemannian manifolds. *Comm. Pure Appl. Math,*, 8(4):551–590, 1955.
[22] M. Gerritsma. Edge functions for spectral element methods. In J. Hesthaven and E. Rønquist, editors, *Spectral and High Order Methods for Partial Differential Equations*, volume 76 of *Springer Lecture Notes in Computational Science and Engineering*, pages 199–208, 2011.
[23] J. Kreeft and M. Gerritsma. Mixed mimetic spectral element method for Stokes flow: A pointwise divergence-free solution. *Journal of Computational Physics*, 240:284–309, 2013.
[24] J. Kreeft, A. Palha, and M. Gerritsma. Mimetic framework on curvilinear quadrilaterals of arbitrary order. *arXiv:1111.4304*, 2011.
[25] A. Lemoine, J.-P. Caltagirone, M. Azaïez, and S. Vincent. Discrete Helmholtz-Hodge decomposition on polyhedral meshes using compatible discrete operators. *Journal of Scientific Computing*, In Press, 2014.
[26] K. Lipnikov, G. Manzini, and M. Shashkov. Mimetic finite difference method. *Journal of Computational Physics*, 254:1163–1227, 2014.
[27] A. Palha, P. Rebelo, R. Hiemstra, J. Kreeft, and M. Gerritsma. Physics-compatible discretization techniques on single and dual grids, with application to the Poisson equation for volume forms. *Journal of Computational Physics*, 257:1394–1422, 2014.
[28] F. Rapetti and A. Bossavit. Geometrical localisation of the degrees of freedom for Whitney elements of higher order. *Science, Measurement Technology, IET*, 1(1):63–66, January 2007.
[29] G. Schwarz. *Hodge Decomposition – A Method for Solving Boundary Value Problems*. Springer Verlag, 1995.
[30] M. Seslija, A. van der Schaft, and J. Scherpen. Discrete exterior geometry approach to structure-preserving discretization of distributed port-Hamiltonian systems. *Journal of Geometry and Physics*, 62(6):1509–1531, 2012.
[31] E. Tonti. On the formal structure of physical theories. *preprint of the Italian National Research Council*, 1975.
[32] E. Tonti. *The Common Structure of Physical Theories*. Springer, 2013.

Delft University of Technology, Faculty of Aerospace Engineering,
Kluyverweg 2, 2629 HT Delft, The Netherlands.
E-mail address: pbboche@sandia.gov, M.I.Gerritsma@TUDelft.nl

Sandia National Laboratories,
Center for Computing Research, Mail Stop 1320, Albuquerque, NM 87185, USA